



## Promoting the interfacial H<sub>2</sub>-evolution reaction of metallic Ag by Ag<sub>2</sub>S cocatalyst: A case study of TiO<sub>2</sub>/Ag-Ag<sub>2</sub>S photocatalyst



Huogen Yu<sup>a,b,\*</sup>, Wenjing Liu<sup>b</sup>, Xuefei Wang<sup>b</sup>, Fazhou Wang<sup>a</sup>

<sup>a</sup> State Key Laboratory of Silicate Materials for Architectures, Wuhan University of Technology, Wuhan, 430070, PR China

<sup>b</sup> School of Chemistry, Chemical Engineering and Life Sciences, Wuhan University of Technology, Wuhan, 430070, PR China

### ARTICLE INFO

#### Keywords:

Photocatalytic H<sub>2</sub> evolution  
Cocatalyst  
Ag-Ag<sub>2</sub>S  
Synergistic effect  
Active sites

### ABSTRACT

Metallic Ag has been widely demonstrated to be an excellent oxygen-reduction cocatalyst to significantly improve the photocatalytic decomposition performance of various organic substances. However, as a H<sub>2</sub>-evolution cocatalyst, the improved photocatalytic performance by metallic Ag is quite limited due to its low H<sub>2</sub>-evolution rate. In this study, for the well-known TiO<sub>2</sub>/Ag photocatalyst, Ag<sub>2</sub>S as the efficient H<sub>2</sub>-evolution active sites was selectively loaded on the metallic Ag surface to greatly promote the interfacial H<sub>2</sub>-evolution reaction rate. In this case, the TiO<sub>2</sub>/Ag-Ag<sub>2</sub>S sample was synthesized by a two-step process including the simple photoinduced deposition of metallic Ag on the TiO<sub>2</sub> surface and the following in situ sulfidation of partial Ag into Ag<sub>2</sub>S. Photocatalytic experimental results indicated that the TiO<sub>2</sub>/Ag-Ag<sub>2</sub>S(40uL) photocatalysts clearly exhibited a significantly higher UV-light photocatalytic H<sub>2</sub>-evolution activity (119.11 μmol h<sup>-1</sup>) than the pure TiO<sub>2</sub>, TiO<sub>2</sub>/Ag and TiO<sub>2</sub>/Ag<sub>2</sub>S photocatalysts by a factor of 51.8, 3.9 and 3.6 times, respectively. On the basis of the present results, a synergistic effect of dual electron-cocatalyst (metallic Ag and Ag<sub>2</sub>S) is proposed for the improved photocatalytic H<sub>2</sub>-evolution activity, namely, the Ag-nanoparticle cocatalyst can steadily capture and transfer the photogenerated electrons from TiO<sub>2</sub> surface, while the Ag<sub>2</sub>S cocatalyst is considered to be the interfacial active sites to promote the rapid H<sub>2</sub>-evolution reaction. This research may provide new strategies for the development of highly efficient photocatalytic materials used in various fields.

### 1. Introduction

Research interest in semiconductor photocatalysts has increased greatly due to their potential applications in solving energy and environment problems [1–6]. Among various semiconductor photocatalysts, TiO<sub>2</sub> is one of the most well-known and excellent photocatalytic materials due to its excellent chemical properties, good stability, and non-toxic harmless [7,8]. However, the pure TiO<sub>2</sub> usually exhibits a limited photocatalytic activity owing to the rapid recombination of photogenerated electrons and holes in the bulk or on its surface [9]. To improve the photocatalytic performance of TiO<sub>2</sub>, various strategies have been widely developed such as semiconductor coupling [10–13], doping with a foreign element [14–16], and surface modification [17–19]. Among them, surface modification with various cocatalysts is one of the most effective methods to enhance its photocatalytic performance of TiO<sub>2</sub> by inhibiting the rapid recombination of photogenerated electron-hole pairs and providing effective active sites to promote their interfacial catalytic reactions. Moreover, cocatalyst modification is usually performed in a mild experimental condition,

thus the crystal structure of host photocatalysts can be well maintained. In addition, the photocatalytic activity of host photocatalysts can be greatly improved by loading a small amount of cocatalysts. Therefore, cocatalyst modification is regarded as an important and effective method to boost up the photocatalytic activity of photocatalysts.

Noble metals (such as Pt [20], Au [21,22] and Pd [23]) have been extensively used as the well-known surface modifier (or electron cocatalyst) to improve the photocatalytic performance of TiO<sub>2</sub> and other photocatalysts. However, their rarity and high cost seriously restrict their wide applications in various fields. For this reason, it is quite significant for us to explore novel, low-cost and earth-abundance cocatalysts to make the solar hydrogen evolution more practical. In this case, silver with a far lower cost than Pt (about 70 times lower than Pt), has attracted extensive attention due to its excellent conductivity and strong electron-trapping ability (Fig. 1a) [24,25]. In fact, Ag has been widely demonstrated to be an efficient electron cocatalyst (or oxygen-reduction cocatalyst) to significantly improve the photocatalytic decomposition rate for various organic substances (Fig. 1b) [26–28]. However, compared with the large amount of investigations for the

\* Corresponding author at: State Key Laboratory of Silicate Materials for Architectures, Wuhan University of Technology, Wuhan, 430070, PR China.  
E-mail address: [yuhogen@whut.edu.cn](mailto:yuhogen@whut.edu.cn) (H. Yu).

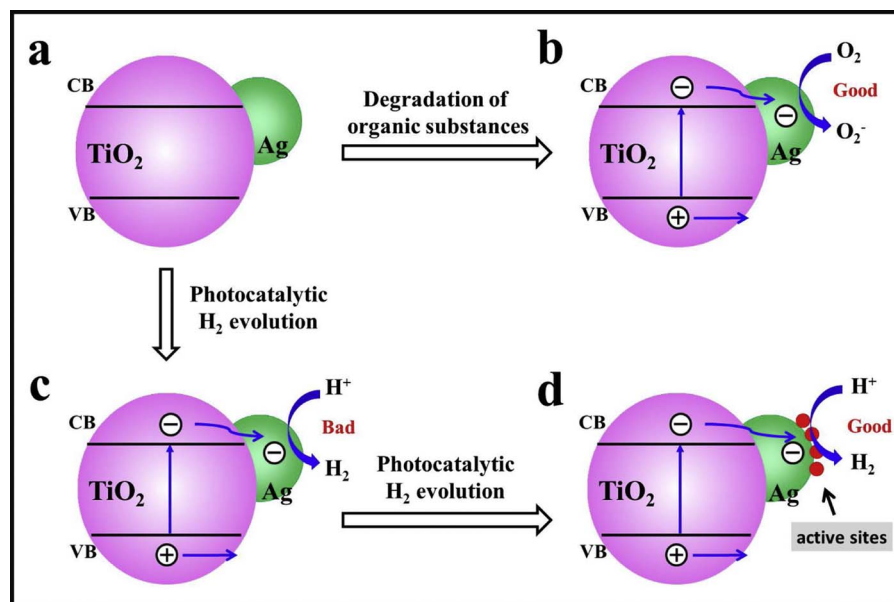


**Fig. 1.** Schematic diagram illustrating the applications of  $\text{TiO}_2/\text{Ag}$  photocatalysts: (a)  $\text{TiO}_2/\text{Ag}$ ; (b) high photocatalytic activity of  $\text{TiO}_2/\text{Ag}$  for the photocatalytic degradation of organic substances; (c) low photocatalytic activity of  $\text{TiO}_2/\text{Ag}$  for photocatalytic  $\text{H}_2$  evolution; (d) surface modification of metallic Ag for the improved photocatalytic  $\text{H}_2$ -evolution of  $\text{TiO}_2/\text{Ag}$ .

oxygen-reduction cocatalyst, the number of metallic Ag as  $\text{H}_2$ -evolution cocatalyst is still quite limited due to its low interfacial  $\text{H}_2$ -evolution reaction (Fig. 1c) [29]. In fact, it has been reported that Ag cannot work as the efficient active site to rapidly capture protons from solution because the bond strength of Ag-H (37 kcal/mol) is much weaker than that of Pt-H (60 kcal/mol) [30]. Recently, Choi et al. reported that the photocatalytic  $\text{H}_2$ -evolution activity of  $\text{Ag}/\text{TiO}_2$  could be obviously improved by selectively absorbing thiocyanate ions which can enhance the transfer rate of interfacial electrons and facilitate the reduction of adsorbed protons (Fig. 1d) [31]. However, the facile, available and effective methods for the improved interfacial  $\text{H}_2$ -evolution rate of metallic Ag are still very scarce. Therefore, it is quite necessary and worthwhile to develop new and facile strategy to further modify Ag surface to achieve a high photocatalytic  $\text{H}_2$ -evolution activity (Fig. 1d).

In this study,  $\text{Ag}_2\text{S}$  as the interfacial active sites was in situ selectively loaded on the metallic Ag surface to greatly promote the interfacial  $\text{H}_2$ -evolution reaction of  $\text{TiO}_2/\text{Ag}$  photocatalysts (denoted as  $\text{TiO}_2/\text{Ag}-\text{Ag}_2\text{S}$ ). In this case, the  $\text{TiO}_2/\text{Ag}-\text{Ag}_2\text{S}$  sample was synthesized by a two-step process including the simple photoinduced deposition of metallic Ag on the  $\text{TiO}_2$  surface and the following in situ sulfidation of partial Ag into  $\text{Ag}_2\text{S}$ . It was found that the photocatalytic  $\text{H}_2$ -evolution activity of  $\text{TiO}_2/\text{Ag}-\text{Ag}_2\text{S}$  was clearly higher than that of pure  $\text{TiO}_2$ ,  $\text{TiO}_2/\text{Ag}$  and  $\text{TiO}_2/\text{Ag}_2\text{S}$  photocatalysts. On the basis of the above experimental results, a possible synergistic effect mechanism of metallic Ag and  $\text{Ag}_2\text{S}$  was proposed to account for the improved photocatalytic  $\text{H}_2$ -evolution activity of  $\text{TiO}_2/\text{Ag}-\text{Ag}_2\text{S}$ . To the best of our knowledge, this is the first report about the enhanced photocatalytic  $\text{H}_2$ -evolution activity of  $\text{TiO}_2/\text{Ag}$  by in situ loading  $\text{Ag}_2\text{S}$  (as interfacial active sites) on metallic Ag surface. The present research may open new opportunities to develop highly efficient photocatalytic materials for energy and environmental applications.

## 2. Experimental section

### 2.1. Preparation of $\text{TiO}_2$ photocatalyst

$\text{TiO}_2$  was synthesized by a simple hydrolysis-calcination method. Briefly, 70 mL of tetrabutyl titanate ( $\text{Ti}(\text{OC}_4\text{H}_9)_4$ , TBOT) was added dropwise into 1000 mL of deionized water (60 °C) for the effective hydrolysis to produce amorphous  $\text{TiO}_2$ . After continuously stirring for 2 h, the obtained white precipitate was washed with deionized water, and then dried at 60 °C for overnight. The above powder was further

calcined at 550 °C for 4 h to obtain the anatase  $\text{TiO}_2$  photocatalyst, which will be used for the following preparation of Ag-modified  $\text{TiO}_2$ .

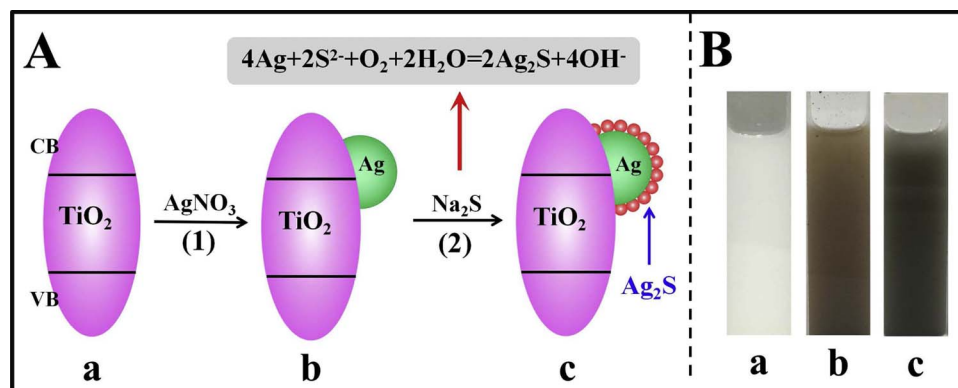
### 2.2. Preparation of $\text{Ag}/\text{TiO}_2$ photocatalyst

Ag nanoparticles were loaded on the  $\text{TiO}_2$  surface to prepare the  $\text{TiO}_2/\text{Ag}$  photocatalyst by a typical photodeposition method, as reported in previous studies [32–34]. First, the obtained  $\text{TiO}_2$  (50 mg) powder was dispersed into 80 mL of aqueous solution with 10 vol% of methyl alcohol, and then 139  $\mu\text{L}$  of  $\text{AgNO}_3$  solution (0.1  $\text{mol L}^{-1}$ ) was injected quickly, where the amount of metallic Ag to  $\text{TiO}_2$  is controlled to be 3 wt%. After stirred vigorously for 1 h to achieve adsorption-desorption equilibrium, the above suspension solution was bubbled with nitrogen for 15 min to remove the dissolved oxygen. Subsequently, the sample was irradiated by UV-light irradiation (3 W, 365 nm, Shenzhen LAMPLIC Science Co. Ltd., China) for 1 h to induce the deposition of metallic Ag nanoparticles on  $\text{TiO}_2$  surface. Finally, the products were centrifuged and washed repeatedly with deionized water, and then dried at 60 °C to obtain the  $\text{TiO}_2/\text{Ag}$  photocatalyst.

### 2.3. Preparation of $\text{TiO}_2/\text{Ag}-\text{Ag}_2\text{S}$ photocatalysts

$\text{Ag}_2\text{S}$  as the interfacial active sites was selectively loaded on the metallic Ag surface via a facile in situ sulfidation of Ag into  $\text{Ag}_2\text{S}$ . In briefly, 50 mg of  $\text{TiO}_2/\text{Ag}$  powder was dispersed into 25 mL of  $\text{H}_2\text{O}$ , and then a certain amount (0–0.24 mL) of sodium sulfide solution (0.1  $\text{mol L}^{-1}$ ) was injected quickly. After strongly stirring for 1 h and then aging for overnight, the above sample was washed with distilled water and dried at 60 °C to obtain the  $\text{TiO}_2/\text{Ag}-\text{Ag}_2\text{S}$  photocatalysts. To investigate the effect of  $\text{S}^{2-}$  amount on the photocatalytic performance of  $\text{Ag}/\text{TiO}_2$  photocatalyst, the dosage of  $\text{Na}_2\text{S}$  solution was controlled to be 0, 8, 24, 40, 80 and 240  $\mu\text{L}$ , and the resulting samples were denoted as  $\text{TiO}_2/\text{Ag}-\text{Ag}_2\text{S}(X\mu\text{L})$ , where X refers to the dosage of  $\text{Na}_2\text{S}$  solution.

For comparison,  $\text{Ag}_2\text{S}$ -modified  $\text{TiO}_2$  photocatalyst ( $\text{TiO}_2/\text{Ag}_2\text{S}$ ) was also prepared by the initial formation of  $\text{Ag}^{+}$ -adsorbed  $\text{TiO}_2$  ( $\text{TiO}_2/\text{Ag}^{+}$ ) and its following transformation to  $\text{TiO}_2/\text{Ag}_2\text{S}$  via the addition of  $\text{Na}_2\text{S}$  solution. First, the preparation progress of  $\text{TiO}_2/\text{Ag}^{+}$  was similar to that of  $\text{TiO}_2/\text{Ag}$  sample in addition to the absence of UV-light irradiation. The transformation progress of  $\text{TiO}_2/\text{Ag}^{+}$  to  $\text{TiO}_2/\text{Ag}_2\text{S}$  was also similar to that of  $\text{TiO}_2/\text{Ag}-\text{Ag}_2\text{S}(40\mu\text{L})$  photocatalyst.



#### 2.4. Characterization

The crystal structure and phase composition of samples were analyzed by a D/MAXRBX X-ray diffractometer (Rigaku Company, Japan). The surface morphology was studied by a JEM-7500F field emission scanning electron microscopy (FESEM, JROL, Japan) equipped with an X-Max 50 energy-dispersive X-ray spectrometer (EDX, Oxford Instruments, Britain). Further morphologies and structural features were based on transmission electron microscopy (TEM) with high-resolution transmission electron microscopy (HRTEM) and high angle annular dark field (HAADF) by using an electron microscope (Titan™ themis 200, FEI, US). Moreover, EDS mapping was acquired with an energy dispersive X-ray spectrometer (EDS) fitted on the microscope. X-ray photoelectron spectroscopy (XPS) measurements were done on a KRATOA XSAM800 XPS system with Mg K $\alpha$  source. All the binding energies were referenced to the C 1s peaks at 284.8 eV for the surface adventitious carbon. UV-vis spectrophotometer (UV-2450, Shimadzu, Japan) was used to obtain the UV-vis absorption spectra with BaSO<sub>4</sub> as the reflectance standard.

#### 2.5. Photocatalytic H<sub>2</sub> production activity

The photocatalytic H<sub>2</sub>-production activity of the samples was evaluated by testing hydrogen production rate in the photocatalytic process, similar to our previous report [35]. The specific experimental procedures were shown as follows: 50 mg of photocatalyst was dispersed in a 100 mL of three-necked Pyrex flask equipped with 80 mL of methyl alcohol solution (10 vol%) at room temperature. Before each experiment, the system was bubbled with nitrogen for 15 min to remove the dissolved oxygen and then the outlets of the flask were sealed with a sealing film. Four low-power LEDs (3 W, 365 nm, Shenzhen Lamplic Science Co. Ltd.) were served as the irradiation light source to trigger the photocatalytic reaction. The focused intensity on the flask for each UV-LED was ca. 80.0 mW cm<sup>-2</sup>. During UV-light irradiation, continuous stirring was applied to keep the photocatalyst particles in suspension state. Finally, gas (0.4 mL) was intermittently sampled through a septum, and hydrogen was analyzed by a gas chromatograph (Shimadzu GC-2014C, Japan, with nitrogen as a carrier gas) equipped with a 5 Å molecular sieve column and a thermal conductivity detector.

#### 2.6. Photoelectrochemical measurements

Photoelectrochemical (PEC) measurements were measured on an electrochemical workstation (CHI660E) in a standard three-electrode configuration with a platinum wire as the counter electrode, standard Ag/AgCl electrode as the reference electrode, and Na<sub>2</sub>SO<sub>4</sub> (0.5 M) aqueous solution as the electrolyte. Before the measurements, this system was continuously purged with N<sub>2</sub> for moving O<sub>2</sub>. The light source was provided by one 3-W LED (365-nm light source with an 80 mW cm<sup>-2</sup>). The working electrodes were prepared on fluorine-

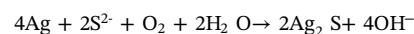
Fig. 2. (A) Schematic diagram illustrating the controllable preparation of the photocatalysts and (B) their corresponding photographs for (a) TiO<sub>2</sub>, (b) TiO<sub>2</sub>/Ag prepared by photoinduced deposition method, and (c) TiO<sub>2</sub>/Ag-Ag<sub>2</sub>S(40 μL) prepared by in situ sulfidation method.

doped tin oxide (FTO) conductor glass. First, FTO glass was washed with deionized water and ethanol for three times, respectively, and then was dried at 60 °C for 3 h. Second, 1 mL of catalyst-ethanol solution (4 mg/mL) and 1 mL of Nafion-ethanol solution (1 wt%) were mixed and then ultrasonically dispersed to form a homogeneous suspension. Finally, the suspension was spread on the FTO glass with the side protected by Scotch tape and dried at 60 °C for 12 h. Linear sweep voltammetry (LSV) was measured in the range of -0.4 to -1.4 V bias (vs Ag/AgCl), and the transient photocurrent responses with time (*i*-*t* curve) was measured at a bias potential of +0.5 V during repeated ON/OFF illumination cycles. For the electrochemical impedance spectroscopy (EIS), it was measured in the frequency range of 0.001–10<sup>6</sup> Hz with an ac amplitude of 10 mV at the open circuit voltage.

### 3. Results and discussion

#### 3.1. Synthesis strategy of TiO<sub>2</sub>/Ag-Ag<sub>2</sub>S photocatalyst

The synthetic procedure of TiO<sub>2</sub>/Ag-Ag<sub>2</sub>S photocatalyst can be schematically illustrated through a facile photoinduced deposition of metallic Ag on the TiO<sub>2</sub> surface and the following in situ sulfidation of partial Ag into Ag<sub>2</sub>S, as shown in Fig. 2. First, the as-prepared TiO<sub>2</sub> powder (Fig. 2A-a) was dispersed into methyl-alcohol solution to form white suspension solution (Fig. 2B-a). After the addition of AgNO<sub>3</sub> solution and under UV-light irradiation, the metallic Ag nanoparticles can be gradually produced on the TiO<sub>2</sub> surface via a photoinduced deposition progress (Fig. 2A-b). In this case, the white TiO<sub>2</sub> suspension clearly becomes a grey color (Fig. 2B-b), indicating the successful deposition of metallic Ag nanoparticles. After washed with deionized water, the resultant TiO<sub>2</sub>/Ag sample was re-dispersed into a Na<sub>2</sub>S solution and kept in the atmosphere condition. During stirring and aging progress, the metallic Ag nanoparticles can be in situ oxidized to produce Ag<sub>2</sub>S by an in situ sulfidation method (Fig. 2A-c), which is shown as follows [36–39]:



Owing to the formation of a dark-brown color of Ag<sub>2</sub>S phase, it is very clear that the final TiO<sub>2</sub>/Ag-Ag<sub>2</sub>S sample shows a brown color (Fig. 2B-c). In addition, the Ag<sub>2</sub>S amount in the TiO<sub>2</sub>/Ag-Ag<sub>2</sub>S samples can be well adjusted by the addition of Na<sub>2</sub>S solution (shown below). Moreover, according to the in situ sulfidation mechanism, the Ag<sub>2</sub>S can only be produced on the metallic Ag surface. Therefore, it is quite believed that the TiO<sub>2</sub>/Ag-Ag<sub>2</sub>S photocatalyst can be easily prepared by the above facile and mild solution route.

#### 3.2. Morphology and microstructures of TiO<sub>2</sub>/Ag-Ag<sub>2</sub>S photocatalysts

The successful synthesis of TiO<sub>2</sub>/Ag-Ag<sub>2</sub>S photocatalysts can be well demonstrated by the following XRD, SEM and TEM results. Fig. 3 shows the XRD patterns of TiO<sub>2</sub>, TiO<sub>2</sub>/Ag, and TiO<sub>2</sub>/Ag-Ag<sub>2</sub>S samples. It is

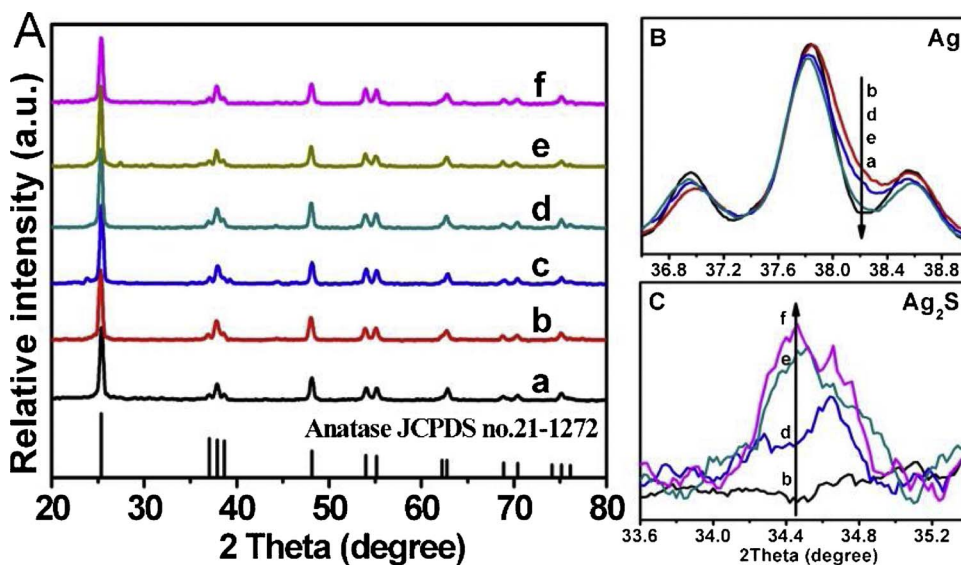


Fig. 3. (A) XRD patterns and the typical diffraction peaks of (B) metallic Ag and (C) Ag<sub>2</sub>S phases for various samples: (a) TiO<sub>2</sub>, (b) TiO<sub>2</sub>/Ag, (c) TiO<sub>2</sub>/Ag-Ag<sub>2</sub>S(8 μL), (d) TiO<sub>2</sub>/Ag-Ag<sub>2</sub>S(40 μL), (e) TiO<sub>2</sub>/Ag-Ag<sub>2</sub>S(80 μL), and (f) TiO<sub>2</sub>/Ag-Ag<sub>2</sub>S(240 μL).

Table 1

The volume of Na<sub>2</sub>S solution added, and the Ag percentages of the metallic Ag and Ag<sub>2</sub>S for different sample.

No.	Sample	The amount of Na <sub>2</sub> S solution (μL)	Ag percentages of metallic Ag (wt%)	Ag percentages of Ag <sub>2</sub> S (wt%)
a	TiO <sub>2</sub>	0	0	0
b	Ag/TiO <sub>2</sub>	0	3	0
c	TiO <sub>2</sub> /Ag-Ag <sub>2</sub> S(8 μL)	8	2.65	0.35
d	TiO <sub>2</sub> /Ag-Ag <sub>2</sub> S(40 μL)	40	1.27	1.73
e	TiO <sub>2</sub> /Ag-Ag <sub>2</sub> S(80 μL)	80	0	3
f	TiO <sub>2</sub> /Ag-Ag <sub>2</sub> S(240 μL)	240	0	3

found that all the resulting samples mainly consist of well-crystallized anatase TiO<sub>2</sub> (JCPDS 21–1272). For the TiO<sub>2</sub>/Ag and TiO<sub>2</sub>/Ag-Ag<sub>2</sub>S samples, their diffraction-peak intensity and full width at half maximum (FWHM) have no obvious change compared with the pure TiO<sub>2</sub>, indicating that the crystal structure of TiO<sub>2</sub> cannot be affected by the cocatalyst loading due to their mild synthetic conditions. Moreover, there are two faint diffraction peaks at ca. 38.2° (Fig. 3B) and ca. 34.47° (Fig. 3C), which can be indexed to the metallic Ag and Ag<sub>2</sub>S phases [40,41], respectively. In addition, with the increase of Na<sub>2</sub>S solution, the peak intensity of metallic Ag gradually decreases while that of Ag<sub>2</sub>S phase gradually increases, strongly suggesting the in situ sulfidation (or in situ transformation) of metallic Ag into Ag<sub>2</sub>S (Fig. 2). To further reveal the sulfidation progress of Ag into Ag<sub>2</sub>S, the Ag-element percentages (compared to the TiO<sub>2</sub> amount) in the metallic Ag and Ag<sub>2</sub>S can be calculated via their XRD peaks, and their results are shown in Table 1. It is found that for the TiO<sub>2</sub>/Ag-Ag<sub>2</sub>S(40 μL), the amounts of Ag and Ag<sub>2</sub>S are 1.27 and 1.73 wt%, respectively. Therefore, the above results clearly suggests the successful preparation of TiO<sub>2</sub>/Ag-Ag<sub>2</sub>S photocatalysts by the present facile solution route.

Fig. 4 illustrates the FESEM images of various TiO<sub>2</sub> photocatalysts. It can be seen that the TiO<sub>2</sub> sample (Fig. 4A) displays an aggregated morphology with a wide size range of 40–60 nm due to a simple calcination method. After loading metallic Ag nanoparticles, the morphology of resultant TiO<sub>2</sub>/Ag (Fig. 4B) shows no significant change compared to that of the pure TiO<sub>2</sub> sample, possibly due to a limited amount of Ag cocatalyst. However, according to the corresponding EDX

data, the Ag element can also be shown in the TiO<sub>2</sub>/Ag photocatalyst in addition to the main Ti and O elements, suggesting the successful loading of metallic Ag. As for the TiO<sub>2</sub>/Ag-Ag<sub>2</sub>S samples (Figs. 4C–D), although they also show a similar surface morphology, the new S signals corresponding to Ag<sub>2</sub>S can be obviously found in their EDX results. In addition, with increasing Na<sub>2</sub>S dosage from 40 to 240 μL, the amount of S in the TiO<sub>2</sub>/Ag-Ag<sub>2</sub>S samples gradually increases from ca. 0.19–0.44 at%, suggesting that in situ sulfidation is an effective method for the transformation of metallic Ag to Ag<sub>2</sub>S. To further explore the morphology and structure of TiO<sub>2</sub>/Ag-Ag<sub>2</sub>S, its corresponding TEM images are shown in Fig. 5A–C. It can be clearly seen that many nanoparticles with a size of about 5–10 nm are homogeneously distributed on the TiO<sub>2</sub> surface (Fig. 5B). HRTEM image indicates that in addition to anatase TiO<sub>2</sub>, the metallic Ag surface is clearly wrapped by a layer of Ag<sub>2</sub>S, which can be further demonstrated by the following elemental-mapping results (Fig. 5D). It is found that the S element is mainly distributed on Ag nanoparticle surface, suggesting that the Ag<sub>2</sub>S has been successfully and selectively loaded on the metallic Ag surface, resulting in the formation of TiO<sub>2</sub>/Ag-Ag<sub>2</sub>S photocatalysts.

The element components and their chemical states of TiO<sub>2</sub>/Ag-Ag<sub>2</sub>S photocatalysts can be provided by XPS. Fig. 6A shows the XPS survey spectra of pure TiO<sub>2</sub>, TiO<sub>2</sub>/Ag and TiO<sub>2</sub>/Ag-Ag<sub>2</sub>S samples. It can be seen that in addition to the C element from the foreign pollution of carbon, all samples show the characteristic peaks of Ti 2p and O 1s, which are ascribed to the TiO<sub>2</sub> phase [32,42]. In addition, compared with the pure TiO<sub>2</sub>, new XPS peaks of Ag 3d can be found in the TiO<sub>2</sub>/Ag and TiO<sub>2</sub>/Ag-Ag<sub>2</sub>S samples, suggesting that the metallic Ag or Ag<sub>2</sub>S has been successfully loaded on the TiO<sub>2</sub> surface. To further observe the chemical information of various elements in the samples, their corresponding high-resolution XPS spectra are shown in Fig. S1 and Figs. 6B–D. Compared with pure TiO<sub>2</sub> with a binding energy of 458.6 eV for Ti 2p<sub>3/2</sub> and 529.8 eV for O 1s (Fig. S1), it can be clearly seen that the XPS peaks of Ti and O elements in TiO<sub>2</sub>/Ag and TiO<sub>2</sub>/Ag-Ag<sub>2</sub>S samples slightly shift to a lower binding energy, in good agreement with the previous study [22]. The high-resolution XPS spectra of Ag 3d and S 2p are shown in Fig. 6B and C, respectively. For the TiO<sub>2</sub>/Ag photocatalyst, there are two individual peaks (367.4 eV and 373.6 eV) in the Ag 3d spectrum (Fig. 6B), which can be assigned to metallic Ag<sup>0</sup> phase [43–45]. With increasing Na<sub>2</sub>S dosage, the XPS peaks of Ag element shift to a higher binding energy (Fig. 6B), which can be attributed to the gradual transformation of metallic Ag to Ag<sub>2</sub>S. As for the XPS spectra of S 2p (Fig. 6C), there is no characteristic peak of S element in the TiO<sub>2</sub>/Ag-Ag<sub>2</sub>S samples when the Na<sub>2</sub>S dosage is lower than 8 μL. Further increasing Na<sub>2</sub>S amount to 40 μL, the S 2p characteristic

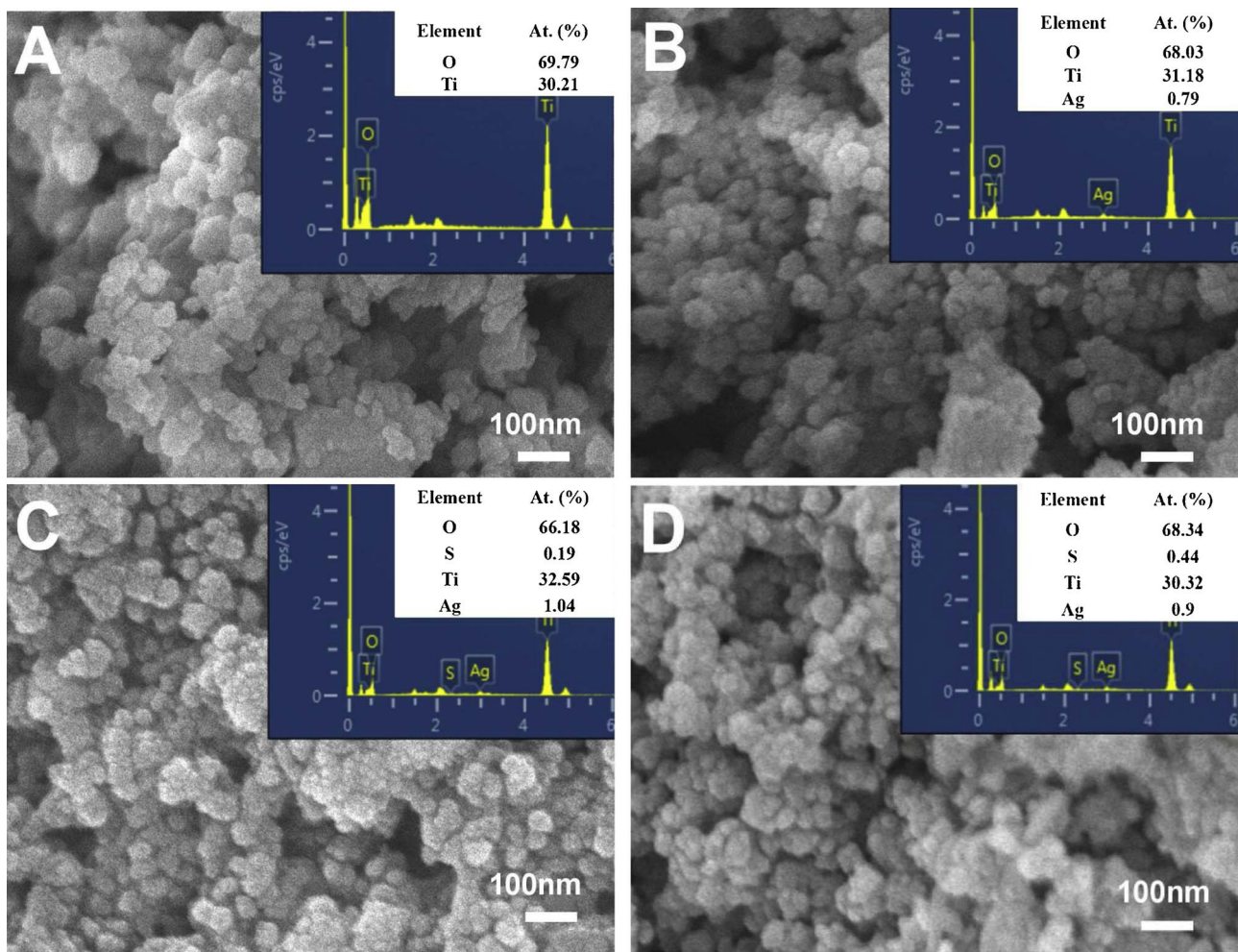


Fig. 4. Typical FESEM/EDS of various samples: (A)  $\text{TiO}_2$ , (B)  $\text{TiO}_2/\text{Ag}$ , (C)  $\text{TiO}_2/\text{Ag}-\text{Ag}_2\text{S}(40 \mu\text{L})$ , and (D)  $\text{TiO}_2/\text{Ag}-\text{Ag}_2\text{S}(240 \mu\text{L})$ .

peak can be clearly observed due to the formation of more  $\text{Ag}_2\text{S}$ . By XPS-peak-differentiation-imitating analysis, it is clear that the S 2p spectra of  $\text{TiO}_2/\text{Ag}-\text{Ag}_2\text{S}$  show two individual peaks at 160.4 eV and 161.6 eV (Fig. 6D), which can be assigned to  $\text{S}^{2-}$  ions in  $\text{Ag}_2\text{S}$  [46,47]. According to Table 2, the amounts of metallic Ag and  $\text{Ag}_2\text{S}$  can be calculated to be 1.4 at% and 0.63 at% in the  $\text{TiO}_2/\text{Ag}-\text{Ag}_2\text{S}(40 \mu\text{L})$  photocatalyst. In addition, to further determine the exact amounts of Ag and  $\text{Ag}_2\text{S}$  on  $\text{TiO}_2$ , inductively coupled plasma-optical emission spectrometry (ICP-OES) was also performed and their corresponding results are shown in Table S1. It is also strongly demonstrated the formation of  $\text{TiO}_2/\text{Ag}-\text{Ag}_2\text{S}$  photocatalyst. Therefore, the above results further strongly demonstrated that the  $\text{Ag}_2\text{S}$  has been successfully loaded on the Ag surface to form  $\text{TiO}_2/\text{Ag}-\text{Ag}_2\text{S}$  photocatalysts.

UV-vis spectra can also show a convincing evidence for the metallic Ag deposition and in situ sulfidation to form  $\text{Ag}_2\text{S}$  on the  $\text{TiO}_2$  surface, as shown in Fig. 7. It can be seen that the absorption boundary of pure  $\text{TiO}_2$  is around 390 nm, which is in line with the well-known band energy of  $\text{TiO}_2$  (ca. 3.2 eV). After the Ag nanoparticles are loaded on the  $\text{TiO}_2$  surface, the resultant  $\text{TiO}_2/\text{Ag}$  exhibits a significantly enhanced visible-light absorption in the range of 390–800 nm owing to the surface plasmon resonance effect of Ag nanoparticles [48,49]. When a small amount of  $\text{Ag}_2\text{S}$  is in situ formed on the Ag surface, the resultant  $\text{TiO}_2/\text{Ag}-\text{Ag}_2\text{S}$  shows an improved visible-light absorption due to the formation of black  $\text{Ag}_2\text{S}$  phase. With further increasing the dosage of  $\text{Na}_2\text{S}$  solution, the plasma-resonance absorption peak of Ag nanoparticles gradually decreases, strongly suggesting the effective transformation from metallic Ag to  $\text{Ag}_2\text{S}$  in the  $\text{TiO}_2/\text{Ag}-\text{Ag}_2\text{S}$  photocatalyst. In addition, the above results can be well explained by their photograph

images (inset in Fig. 7), where the  $\text{TiO}_2/\text{Ag}-\text{Ag}_2\text{S}$  samples gradually become a lighter color with the formation of more  $\text{Ag}_2\text{S}$ .

### 3.3. Photocatalytic performance and mechanism

The photocatalytic  $\text{H}_2$ -production activities of all samples are evaluated by their hydrogen production rate under UV-light irradiation. Fig. 8 shows the photocatalytic  $\text{H}_2$ -production rate of  $\text{TiO}_2$ ,  $\text{TiO}_2/\text{Ag}$ ,  $\text{TiO}_2/\text{Ag}-\text{Ag}_2\text{S}$ , and  $\text{TiO}_2/\text{Ag}_2\text{S}$  samples. It can be seen that the pure  $\text{TiO}_2$  (Fig. 8a) shows a negligible photocatalytic  $\text{H}_2$ -evolution activity ( $2.30 \mu\text{mol h}^{-1}$ ) with a low quantum efficiency (QE) of 0.19%, which is mainly due to the rapid recombination of photogenerated carriers. After surface modification by Ag cocatalyst, the  $\text{H}_2$ -evolution activity of  $\text{TiO}_2/\text{Ag}$  (Fig. 8b) is increased owing to the rapid transfer and separation of photogenerated electrons from  $\text{TiO}_2$  surface to Ag nanoparticles. With further modification of metallic Ag by  $\text{Ag}_2\text{S}$ , all the resultant  $\text{TiO}_2/\text{Ag}-\text{Ag}_2\text{S}$  samples display a significantly improved  $\text{H}_2$ -evolution activity. In particular, the  $\text{TiO}_2/\text{Ag}-\text{Ag}_2\text{S}(40 \mu\text{L})$  exhibits the highest  $\text{H}_2$ -production performance ( $119.11 \mu\text{mol h}^{-1}$ ) with a QE of 9.84%, which is obviously higher than that of pure  $\text{TiO}_2$  and  $\text{TiO}_2/\text{Ag}$  by a factor of 51.8 and 3.9 times, respectively. However, with further increase of the  $\text{Na}_2\text{S}$  dosage ( $> 40 \mu\text{L}$ ), the  $\text{H}_2$ -evolution activity of  $\text{TiO}_2/\text{Ag}-\text{Ag}_2\text{S}$  has a significant decrease. In fact, the  $\text{H}_2$ -evolution activity of  $\text{TiO}_2/\text{Ag}-\text{Ag}_2\text{S}(80 \mu\text{L})$  is comparable to that of  $\text{TiO}_2/\text{Ag}-\text{Ag}_2\text{S}(240 \mu\text{L})$ , which can be attributed to the complete transformation of metallic Ag to  $\text{Ag}_2\text{S}$  according to the XRD results (Table 1).

On the basis of the above-mentioned results, a possible mechanism for the enhanced  $\text{H}_2$ -evolution activity of  $\text{TiO}_2/\text{Ag}-\text{Ag}_2\text{S}$  is proposed and

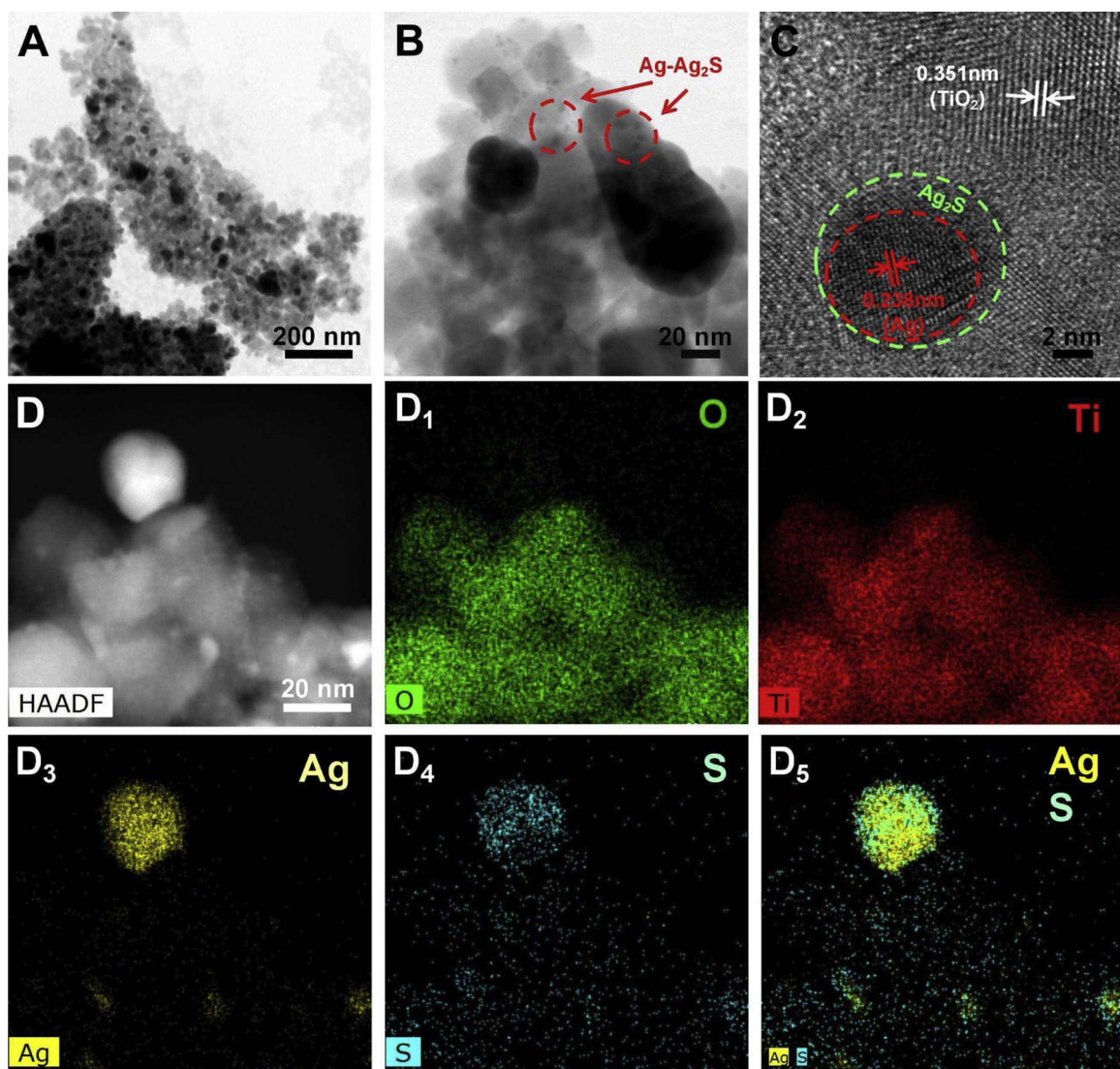


Fig. 5. (A, B) TEM, (C) HRTEM and (D–D5) HAADF-STEM and EDS mapping images of the  $\text{TiO}_2/\text{Ag}-\text{Ag}_2\text{S}$ (40  $\mu\text{L}$ ) photocatalyst.

shown in Fig. 9. For the pure  $\text{TiO}_2$  photocatalyst, its  $\text{H}_2$ -evolution rate is negligible due to the rapid combination of electron-hole pairs. After surface modification by metallic Ag, the  $\text{TiO}_2/\text{Ag}$  exhibits a lightly improved  $\text{H}_2$ -evolution rate owing to the rapid capture and transfer for the photogenerated electrons from the conduction band of  $\text{TiO}_2$ . However, compared with noble metal Pt, metallic Ag cannot work as the effective  $\text{H}_2$ -evolution active site for  $\text{H}^+$  adsorption and its following  $\text{H}_2$  evolution. After selective deposition of  $\text{Ag}_2\text{S}$  on the metallic Ag surface, the  $\text{TiO}_2/\text{Ag}-\text{Ag}_2\text{S}$  clearly shows a remarkably enhanced  $\text{H}_2$ -evolution performance. As a consequence, it is quite believed that the  $\text{Ag}_2\text{S}$  can act as effective catalytic active sites to greatly promote the interfacial  $\text{H}_2$ -evolution reaction of metallic Ag in  $\text{TiO}_2/\text{Ag}-\text{Ag}_2\text{S}$  system. Similar results can also be found in other sulfide cocatalysts. It was reported that many sulfides ( $\text{MoS}_2$  [47,50,51],  $\text{NiS}$  [52,53],  $\text{CoS}$  [54,55] et al.) can work as the interfacial catalytic active sites for photocatalytic  $\text{H}_2$  evolution because their interfacial or unsaturated S atoms can efficiently capture  $\text{H}^+$  ions from solution and then promote the rapid reduction of adsorbed protons to  $\text{H}_2$ , thereby greatly improving the photocatalytic  $\text{H}_2$ -production activity. According to the work function of metallic Ag (-4.26 eV) [56] and the conduction-band potentials of  $\text{TiO}_2$  (-4.21 eV) [57] and  $\text{Ag}_2\text{S}$  (-4.50 eV) [58], an electron-transfer route in the  $\text{TiO}_2/\text{Ag}-\text{Ag}_2\text{S}$  is shown in Fig. 9A. Obviously, the photogenerated electrons on the conduction band of  $\text{TiO}_2$  can easily

transfer to the metallic Ag and then to the  $\text{Ag}_2\text{S}$ . Therefore, for the  $\text{TiO}_2/\text{Ag}-\text{Ag}_2\text{S}$  photocatalysts (Fig. 9B), the synergistic effect mechanism of metallic Ag and  $\text{Ag}_2\text{S}$  contributes to their improved photocatalytic  $\text{H}_2$ -evolution activity, namely, Ag nanoparticles are first used as electron capturers to rapidly capture photogenerated electrons from the  $\text{TiO}_2$  surface (step (1)), and then serve as an electron-transfer mediator to steadily transport electrons to the  $\text{Ag}_2\text{S}$  active sites (step (2)), while the  $\text{Ag}_2\text{S}$  function as interfacial catalytic active-sites to effectively accelerate the interfacial  $\text{H}_2$ -evolution reaction (step (3)).

To demonstrate the above assumption that  $\text{Ag}_2\text{S}$  can work as the effective interfacial catalytic active-site to rapidly promote the interfacial  $\text{H}_2$ -evolution reaction, the PEC measurements were measured in a standard three-electrode configuration by using  $\text{Na}_2\text{SO}_4$  (0.5 M) as the electrolyte. The linear sweep voltammograms (LSV) of various samples were first performed without light irradiation and the results are shown in Fig. 10A. It can be found that compared with the naked  $\text{TiO}_2$ , the metallic Ag modification slightly reduces the overpotential of  $\text{H}_2$  production due to the rapid capture of photogenerated electrons by Ag nanoparticles. When the  $\text{Ag}_2\text{S}$  was further selectively loaded on the metallic Ag surface in the  $\text{TiO}_2/\text{Ag}$  system, the onset potential for  $\text{H}_2$  evolution was further shifted to a more positive potential (hence less overpotential for  $\text{H}_2$  production) and a larger current density could be observed, indicating that the  $\text{Ag}_2\text{S}$  can work as the highly efficient

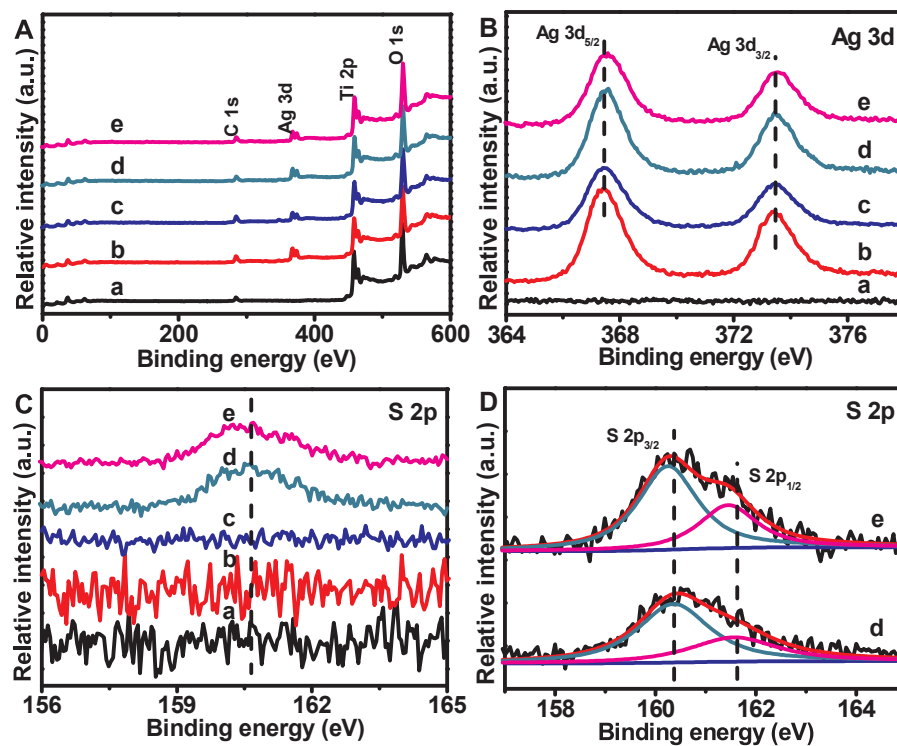


Fig. 6. (A) XPS survey spectra and (B-D) the high-resolution XPS spectra of (B) Ag 3d and (C, D) S 2p for various samples: (a)  $\text{TiO}_2$ , (b)  $\text{TiO}_2/\text{Ag}$ , (c)  $\text{TiO}_2/\text{Ag}-\text{Ag}_2\text{S}(8 \mu\text{L})$ , (d)  $\text{TiO}_2/\text{Ag}-\text{Ag}_2\text{S}(40 \mu\text{L})$ , and (e)  $\text{TiO}_2/\text{Ag}-\text{Ag}_2\text{S}(240 \mu\text{L})$ .

Table 2  
Element components of various samples based on the XPS results.

Sample	Ti	O	Ag	S
$\text{TiO}_2$	27.60	72.40	0	0
$\text{TiO}_2/\text{Ag}$	23.80	72.25	3.95	0
$\text{TiO}_2/\text{Ag}-\text{Ag}_2\text{S}(8 \mu\text{L})$	23.97	73.39	2.64	0
$\text{TiO}_2/\text{Ag}-\text{Ag}_2\text{S}(40 \mu\text{L})$	23.89	72.82	2.66	0.63
$\text{TiO}_2/\text{Ag}-\text{Ag}_2\text{S}(240 \mu\text{L})$	23.93	73.11	1.96	1.00

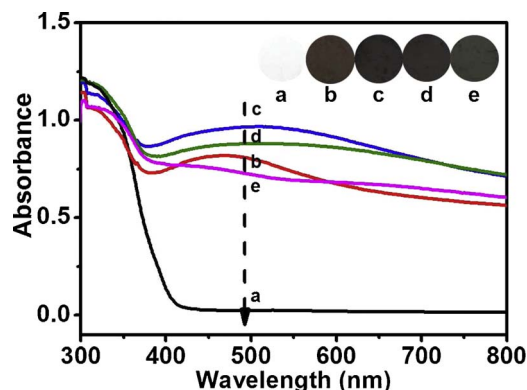


Fig. 7. UV-vis spectra of various samples: (a)  $\text{TiO}_2$ , (b)  $\text{TiO}_2/\text{Ag}$ , (c)  $\text{TiO}_2/\text{Ag}-\text{Ag}_2\text{S}(8 \mu\text{L})$ , (d)  $\text{TiO}_2/\text{Ag}-\text{Ag}_2\text{S}(40 \mu\text{L})$ , and (e)  $\text{TiO}_2/\text{Ag}-\text{Ag}_2\text{S}(240 \mu\text{L})$ .

active sites to greatly promote the interfacial  $\text{H}_2$ -evolution reaction of  $\text{TiO}_2/\text{Ag}$  photocatalysts. To further investigate the capture, separation and transfer efficiency of photogenerated carriers in  $\text{TiO}_2/\text{Ag}-\text{Ag}_2\text{S}$ , the transient photocurrent responses with time ( $i-t$  curve) and electrochemical impedance spectroscopy (EIS) of various photocatalyst are shown in Fig. 10B and C, respectively. Compared with the pure  $\text{TiO}_2$  and  $\text{TiO}_2/\text{Ag}$  photocatalysts, the  $\text{TiO}_2/\text{Ag}-\text{Ag}_2\text{S}$  photocatalyst shows an improved photocurrent density, suggesting that the photogenerated holes in the  $\text{TiO}_2/\text{Ag}-\text{Ag}_2\text{S}$  system can be effectively separated from photogenerated electrons, causing a rapid interfacial catalytic

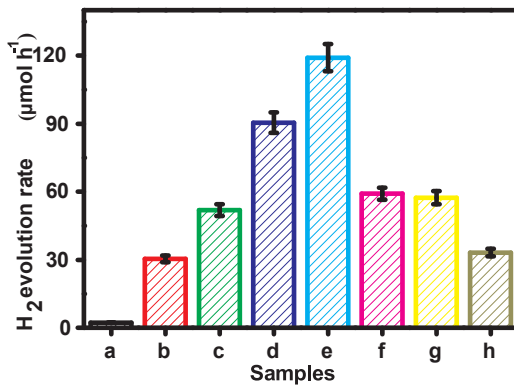
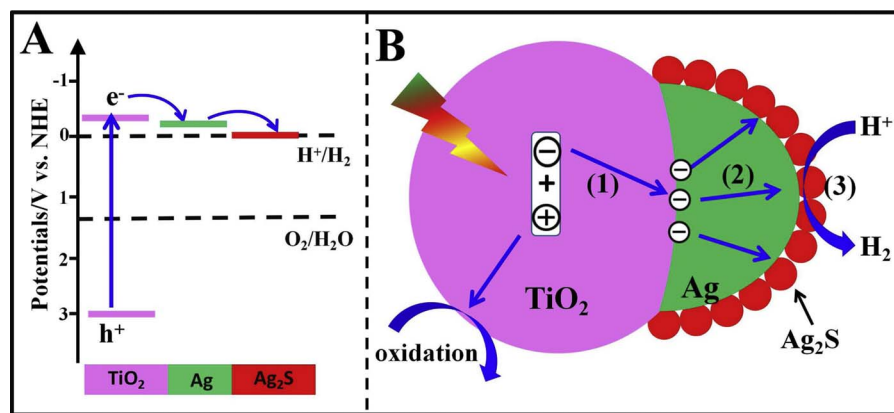


Fig. 8. The photocatalytic  $\text{H}_2$ -production activity of various samples: (a)  $\text{TiO}_2$ , (b)  $\text{TiO}_2/\text{Ag}$ , (c)  $\text{TiO}_2/\text{Ag}-\text{Ag}_2\text{S}(8 \mu\text{L})$ , (d)  $\text{TiO}_2/\text{Ag}-\text{Ag}_2\text{S}(24 \mu\text{L})$ , (e)  $\text{TiO}_2/\text{Ag}-\text{Ag}_2\text{S}(40 \mu\text{L})$ , (f)  $\text{TiO}_2/\text{Ag}-\text{Ag}_2\text{S}(80 \mu\text{L})$ , (g)  $\text{TiO}_2/\text{Ag}-\text{Ag}_2\text{S}(240 \mu\text{L})$ , and (h)  $\text{TiO}_2/\text{Ag}-\text{Ag}_2\text{S}(40 \mu\text{L})$ .

reaction. In addition, the  $\text{TiO}_2/\text{Ag}-\text{Ag}_2\text{S}$  samples show a smaller arc radius on the EIS plots than the  $\text{TiO}_2$  and  $\text{TiO}_2/\text{Ag}$ , suggesting a higher transfer efficiency of photogenerated carriers in the  $\text{TiO}_2/\text{Ag}-\text{Ag}_2\text{S}$  photocatalyst. Therefore, it can be deduced that the excellent synergistic effect of metallic Ag and  $\text{Ag}_2\text{S}$  in the  $\text{TiO}_2/\text{Ag}-\text{Ag}_2\text{S}$  system contribute to the enhanced photocatalytic  $\text{H}_2$ -evolution activity.

#### 4. Conclusions

In summary, the  $\text{Ag}_2\text{S}$  as the interfacial active site has been successfully and selectively loaded on the metallic Ag surface of  $\text{TiO}_2/\text{Ag}$  to prepare the  $\text{TiO}_2/\text{Ag}-\text{Ag}_2\text{S}$  photocatalyst by the in situ sulfidation of metallic Ag into  $\text{Ag}_2\text{S}$ . It can be found that the resultant  $\text{TiO}_2/\text{Ag}-\text{Ag}_2\text{S}$  photocatalyst shows a remarkably higher photocatalytic  $\text{H}_2$ -evolution performance ( $119.11 \mu\text{mol h}^{-1}$ ) than the unmodified  $\text{TiO}_2$  ( $2.30 \mu\text{mol h}^{-1}$ ) and  $\text{TiO}_2/\text{Ag}$  photocatalyst ( $30.43 \mu\text{mol h}^{-1}$ ) by a factor of 51.8 and 3.9 times, respectively. An excellent synergistic effect of metallic Ag and  $\text{Ag}_2\text{S}$  was proposed to account for the improved photocatalytic  $\text{H}_2$ -evolution activity, namely, the Ag nanoparticle can



**Fig. 9.** (A) The energy-band structures of TiO<sub>2</sub>, Ag and Ag<sub>2</sub>S and (B) schematic diagram illustrating the photocatalytic H<sub>2</sub>-evolution mechanism of TiO<sub>2</sub>/Ag-Ag<sub>2</sub>S: (1) the rapid capture of photogenerated electrons by metallic Ag; (2) the effective transfer of photogenerated electrons from the capture sites to active sites by metallic Ag; (3) the efficient interfacial H<sub>2</sub>-evolution reactions on the Ag<sub>2</sub>S active sites.

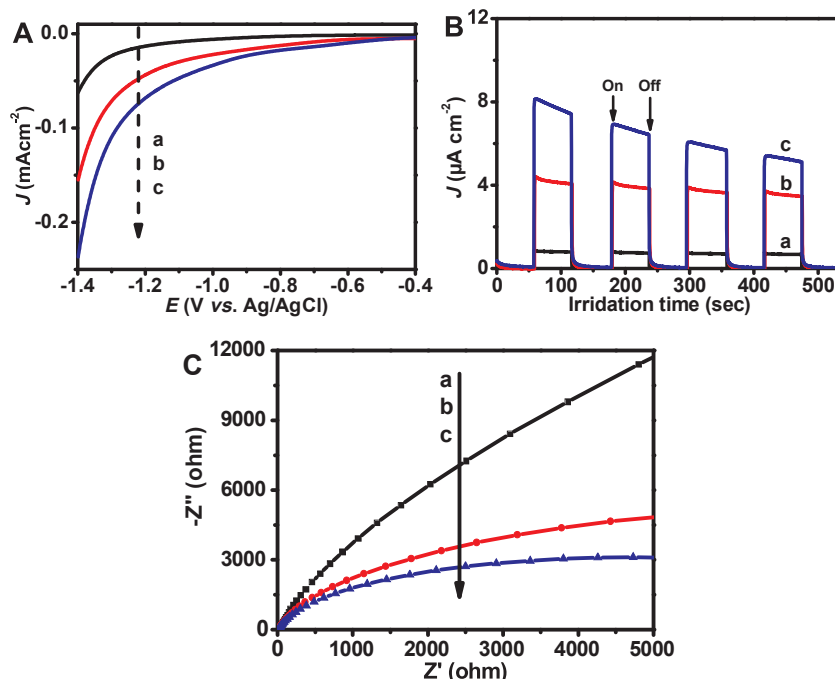


**Fig. 10.** (A) Linear sweep voltammetry (LSV) curves, (B) transient photocurrent responses and (C) electrochemical impedance spectra for various samples: (a) TiO<sub>2</sub>, (b) TiO<sub>2</sub>/Ag, and (c) TiO<sub>2</sub>/Ag<sub>2</sub>S(40 μL).

steadily capture and rapidly transfer the photogenerated electrons from TiO<sub>2</sub> surface, while the Ag<sub>2</sub>S is considered as the interfacial active sites to promote the rapid H<sub>2</sub>-evolution reaction. This research may provide some new strategies to develop highly efficient photocatalytic materials for solving energy and environment problems.

## Acknowledgements

This work was supported by the National Natural Science Foundation of China (51472192, 51672203, 21477094, and 21771142). This work was also financially supported by the Fundamental Research Funds for the Central Universities (WUT 2017IB002).

## Appendix A. Supplementary data

Supplementary data associated with this article can be found, in the online version, at <https://doi.org/10.1016/j.apcatb.2017.12.026>.

## References

- [1] X. Li, J. Yu, J. Low, Y. Fang, J. Xiao, X. Chen, *J. Mater. Chem. A* 3 (2015) 2485–2534.
- [2] Y. Li, Y. Bian, H. Qin, Y. Zhang, Z. Bian, *Appl. Catal. B: Environ.* 206 (2017) 293–299.
- [3] H. Yu, P. Xiao, J. Tian, F. Wang, J. Yu, *ACS Appl. Mater. Interfaces* 8 (2016) 29470–29477.
- [4] W. Wang, M.O. Tade, Z. Shao, *Chem. Soc. Rev.* 44 (2015) 5371–5408.
- [5] S. Song, B. Cheng, N. Wu, A. Meng, S. Cao, J. Yu, *Appl. Catal. B: Environ.* 181 (2016) 71–78.
- [6] X. Qian, D. Yue, Z. Tian, M. Reng, Y. Zhu, M. Kan, T. Zhang, Y. Zhao, *Appl. Catal. B: Environ.* 193 (2016) 16–21.
- [7] C. Luo, X. Ren, Z. Dai, Y. Zhang, X. Qi, C. Pan, *ACS Appl. Mater. Interfaces* 9 (2017) 23265–23286.
- [8] Y. Xu, Y. Mo, J. Tian, P. Wang, H. Yu, J. Yu, *Appl. Catal. B: Environ.* 181 (2016) 810–817.
- [9] A.M. Bakhshayesh, M.R. Mohammadi, D.J. Fray, *Electrochim. Acta* 78 (2012) 384–391.
- [10] J. Li, M. Zhang, Q. Li, J. Yang, *Appl. Surf. Sci.* 391 (2017) 184–193.
- [11] L. Pan, J. Zhang, X. Jia, Y.-H. Ma, X. Zhang, L. Wang, J.-J. Zou, *Chinese J. Catal.* 38 (2017) 253–259.
- [12] G. Yang, D. Chen, H. Ding, J. Feng, J.Z. Zhang, Y. Zhu, S. Hamid, D.W. Bahnemann, *Appl. Catal. B: Environ.* 219 (2017) 611–618.
- [13] Y. Kuwahara, Y. Sumida, K. Fujiwara, H. Yamashita, *ChemCatChem* 8 (2016) 2781–2788.
- [14] M. Xu, P. Da, H. Wu, D. Zhao, G. Zheng, *Nano Lett.* 12 (2012) 1503–1508.
- [15] X. Yan, C. Xue, B. Yang, G. Yang, *Appl. Surf. Sci.* 394 (2017) 248–257.
- [16] R. Liu, P. Wang, X. Wang, H. Yu, J. Yu, *J. Phys. Chem. C* 116 (2012) 17721–17728.
- [17] P. Wang, Y. Lu, X. Wang, H. Yu, *Appl. Surf. Sci.* 391 (2017) 259–266.
- [18] J. Low, B. Cheng, J. Yu, *Appl. Surf. Sci.* 392 (2017) 658–686.
- [19] Q. Xiang, J. Yu, M. Jaroniec, *J. Am. Chem. Soc.* 134 (2012) 6575–6578.
- [20] J. Yang, H. Yan, X. Wang, F. Wen, Z. Wang, D. Fan, J. Shi, C. Li, *J. Catal.* 290 (2012) 151–157.
- [21] G. Zhang, H. Miao, X. Hu, J. Mu, X. Liu, T. Han, J. Fan, E. Liu, Y. Yin, J. Wan, *Appl.*

